Supplementary Material

Trident-shaped Fully 3D-printed Electrochemical Sensor for Real-time Measurements

Martina Tuccillo[1,‡], Panagiota M. Kalligosfyri[1,‡,*], Antonella Miglione[1], Concetta Di Natale[2], Michele Spinelli[3], Angela Amoresano[3], Donato Calabria[4,5], Mara Mirasoli[4,5,6], Ibrahim A. Darwish[7], Stefano Cinti[1,8,9,*]

[1]Department of Pharmacy, University of Naples "Federico II", 80131 Naples, Italy

[2] University of Naples Federico II, Dipartimento di Ingegneria Chimica, dei Materiali e della Produzione Industriale, P.le Tecchio 80, I-80125, Naples, Italy

[3]Department of Chemical Sciences, University of Naples "Federico II", 80126 Naples, Italy

[4]Department of Chemistry "Giacomo Ciamician", Alma Mater Studiorum - University of Bologna, Via Piero Gobetti 85, 40129 Bologna, Italy

[5]Interdepartmental Centre for Industrial Aerospace Research (CIRI AEROSPACE), Alma Mater Studiorum-University of Bologna, Via Baldassarre Canaccini 12, I- 47121, Forlì, Italy [+]

[6]Interdepartmental Centre for Industrial Research in Renewable Resources, Environment, Sea and Energy (CIRI FRAME), Alma Mater Studiorum - University of Bologna, Via Sant'Alberto 163, I-48123, Ravenna, Italy

[7]Department of Pharmaceutical Chemistry, College of Pharmacy, King Saud University, P.O. Box 2457 Riyadh 11451, Saudi Arabia.

[8]Sbarro Institute for Cancer Research and Molecular Medicine, Center for Biotechnology, College of Science and Technology, Temple University, Philadelphia, PA 19122, USA

[9]Bioelectronics Task Force at University of Naples Federico II, Via Cinthia 21, 80126 Naples, Italy

[‡]These authors contributed equally.

[*]Corresponding authors: panagiota.kalligosfyri@unina.it, stefano.cinti@unina.it

3D-printed trident-shaped device and 3D-printed electrodes assembly

The 3D-printed device consisted of a three-electrode system namely the working and counter electrodes fabricated from conductive PLA filament and the reference electrode fabricated by conductive PLA filament and a thin layer of conductive Ag/AgCl conductive ink. The dimensions for the 3D-printed electrodes were the same for all electrodes, i.e. 6 mm width, 2 mm thickness and 30 mm height, as shown in Figure S1A and the Ag/AgCl reference electrode had a height of 5 mm.

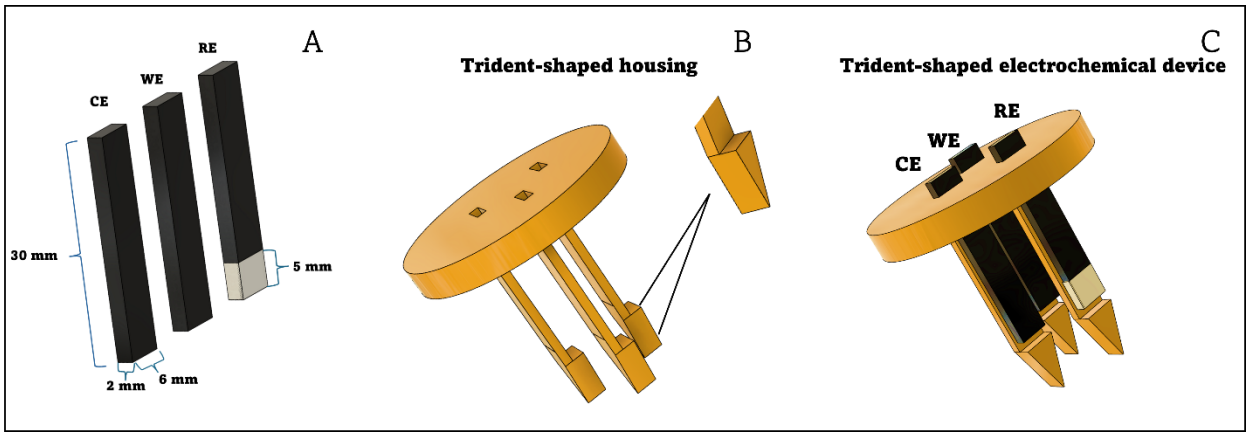

Figure S1. A) Dimensions of the 3D-printed electrodes, B) Trident-shaped housing, C) Assembly of the trident-shaped electrochemical device. CE: Counter electrode, WE: Working electrode, RE: Reference electrode.

The 3D-printed housing for the electrodes was designed to facilitate the easy insertion of the sensing device into the fruit, penetrating the peel (Fig. S1B). Finally, the 3D-printed electrodes were easily inserted into the trident-shaped device through equally sized slits. For analysis, the pins of the electrodes were directly connected to the sensing device.

Optimization studies

Optimization studies were conducted to enhance the performance of 3D-printed electrodes. Cyclic voltammetry (CV) was used to evaluate the working electrode with 5 mM potassium ferricyanide in 1M KCl as the analyte. In the optimization studies of dimensions and infill pattern of the 3D-printed working electrode was assessed by using external screen-printed counter and reference electrodes that were prepared as reported previously.

Pre-treatment step

The pre-treatment step was examined in terms of varying NaOH concentration, due to the effect in electrochemical signal as referenced in previous studies. Comparing the 3D-printed electrodes before and after the pretreatment, it is evident that the NaOH treatment affects the surface of the line-patterned electrodes. As seen in Figures S2A, S2B and S2B, S2F for non-pre-treated and pre-treated 3D electrodes respectively, the linear cavities appear more continuous after the pretreatment step. Additionally, comparing Figure S2D, at a smaller scale of 300 µm, with Figure S2H, the NaOH pretreatment creates deeper hollow regions within the electrode. The NaOH

treatment facilitates the release of the carbon component from the carbon-based PLA conductive filament, making the electrode surface more accessible. This is also supported by the electrochemical measurements (Figure 2A), which show a 2.4-fold increase in current using the optimal 0.5 M of NaOH concentration.

Scanning electron microscopy (SEM) characterization

The 3D-printed electrodes were characterized morphologically by SEM by using the SEM-Hitachi TM3000 configuration.

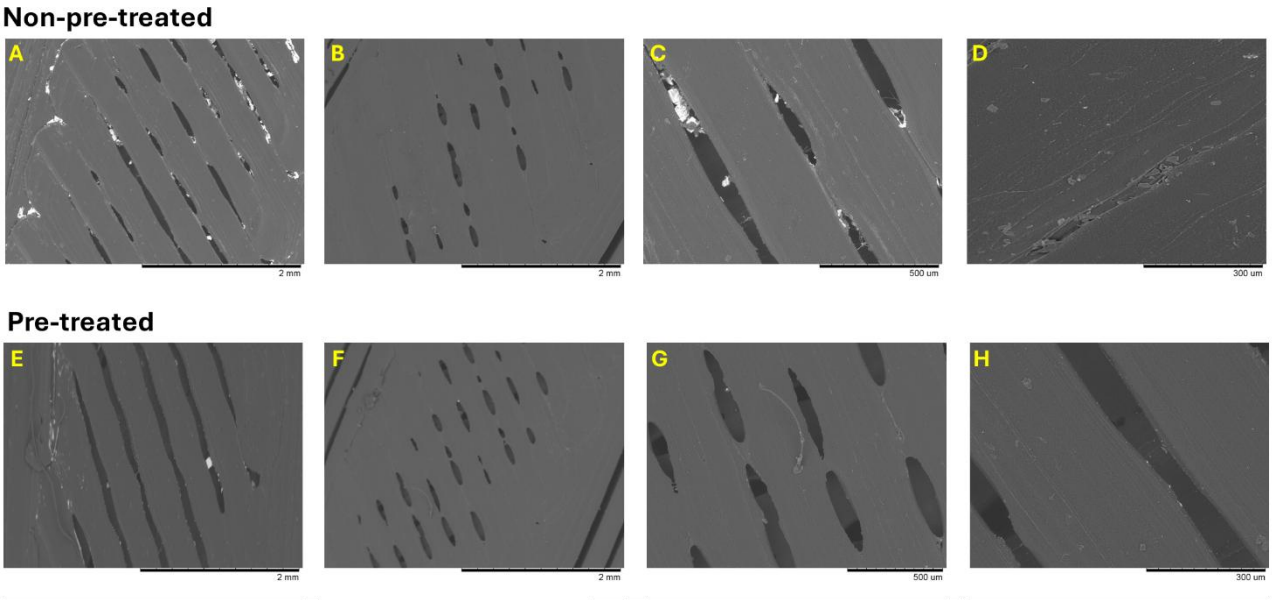

Figure S2. SEM micrographs of the surface of the 3D-printed electrodes before and after the pre-treatment with a 0.5 M NaOH solution. A), B), C), D) show the morphologies of the 3D-printed electrodes before the pre-treatment. E), F), G), H) show the morphologies of the 3D-printed electrodes after the pre-treatment.

Dimensions optimization

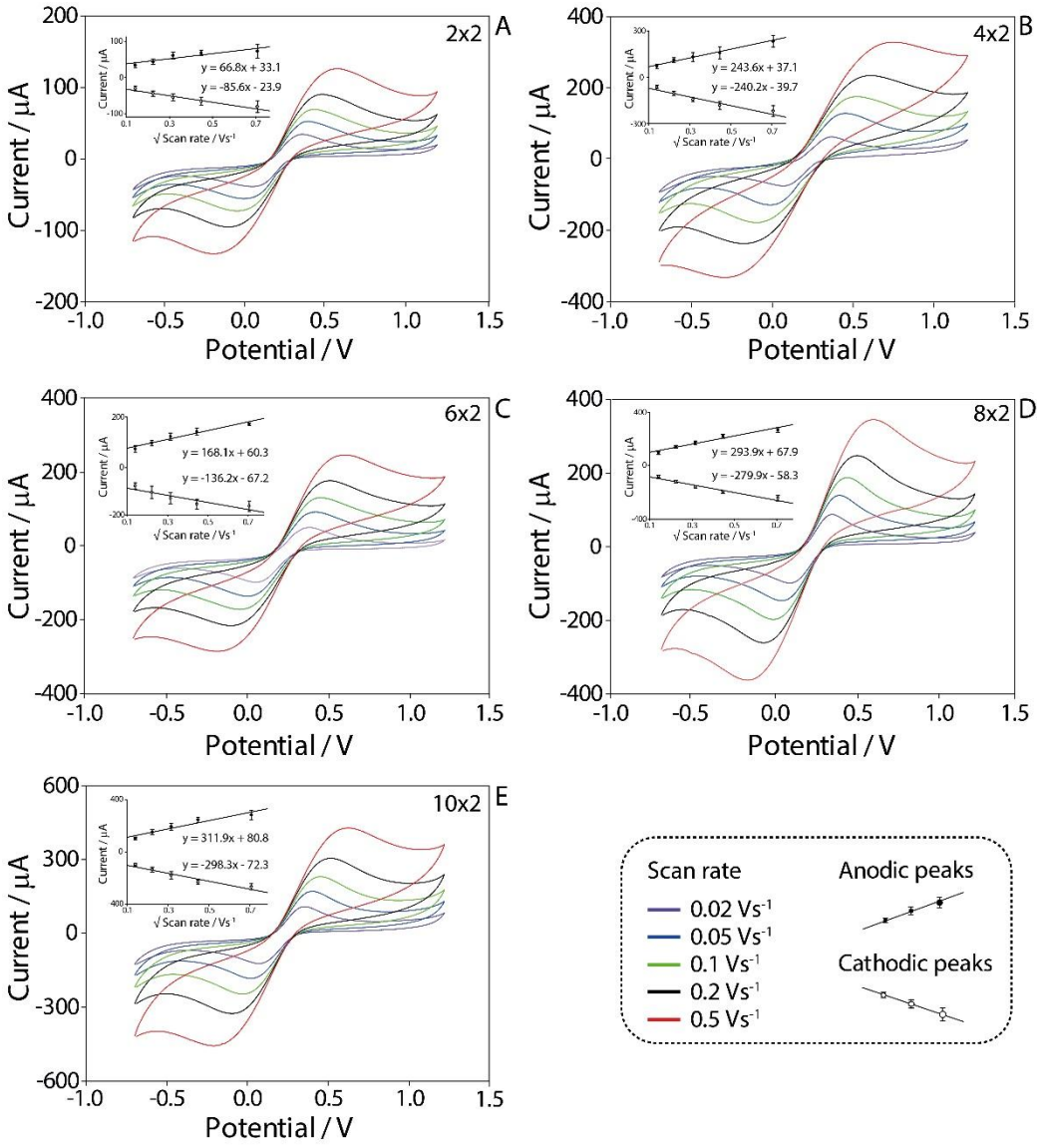

Figure S3. Optimization of the 3D-printed working electrodes width, evaluated at A) 2x2, B) 4x2, C) 6x2, D) 8x2 and E) 10x2 mm. Cyclic voltametric (CV) experiments were recorded for each electrode dimension through the analysis of 1 mL of 5 mM $K_3Fe(CN)_6$ solution, using increasing scan rates from 0.02 to 0.5 Vs^{-1}. Inset: linearity among the intensity of the anodic (solid black circles) and cathodic (empty white circles) and the square root of the tested scan rates. The experiments were performed in 6 replicates.

Printing speed

The printing speed during extrusion was set in the Cura slicer at 80 mm/s, which corresponds to 100% speed. The evaluated percentages and their actual speeds were: 30% (24 mm/s), 50% (40 mm/s), 70% (56 mm/s), and 100% (80 mm/s). To investigate the effect of printing speed on the surface morphology of the electrodes, SEM imaging was performed. At 30%, the slower extrusion led to greater material accumulation, particularly at the edges, resulting in prominent surface irregularities. These features were especially evident within the 2 mm scale region, where raised ridges and edge defects were visible. At 50% and 70%, the surface appeared more uniform, with significantly smaller cavities. In contrast, the 100% speed condition exhibited the largest and most inconsistent defects, as highlighted in red in the SEM images. ImageJ analysis was used to quantify the average diameter of the cavities, revealing median values of 0.23 mm for 30%, 0.09 mm for 50%, 0.04 mm for 70%, and 0.43 mm for 100%. These findings support the rationale for selecting 70% as the optimal printing speed, as it produced a more homogeneous surface with fewer edge defects, leading to improved repeatability in the electrochemical response. This correlation is further reflected in the current intensities and lower standard deviations observed at this speed (Figure S5).

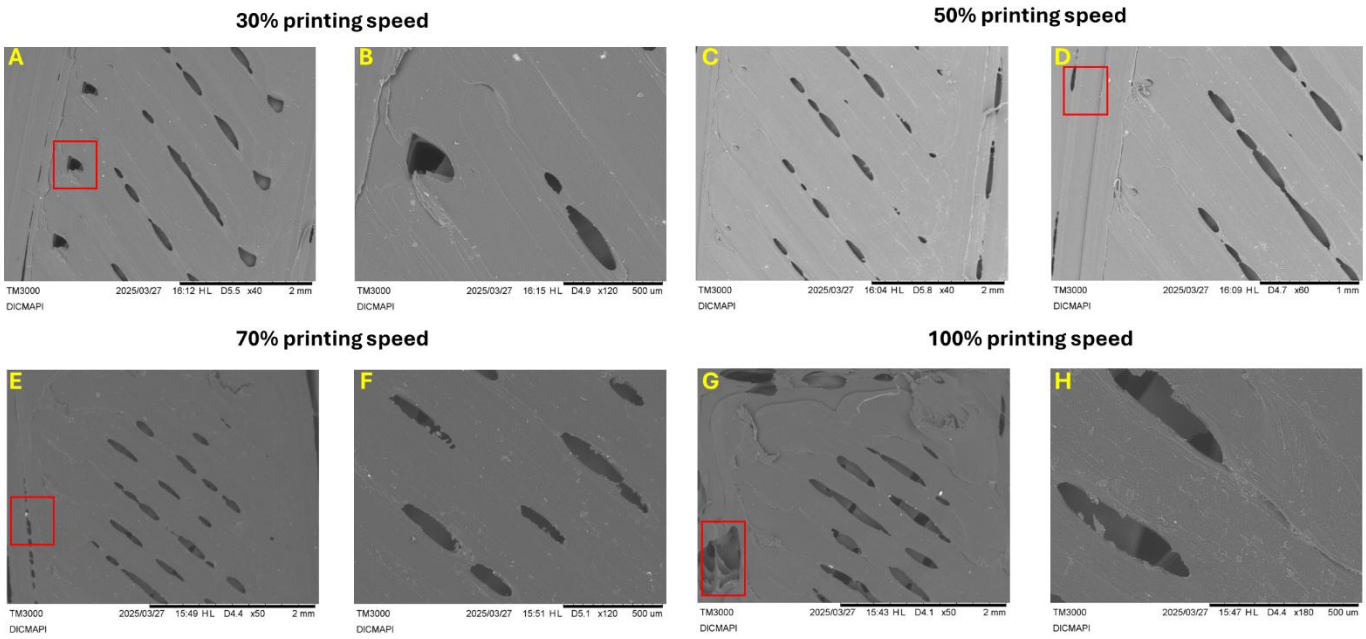

Figure S4. SEM micrographs of 3D-printed electrode surfaces at various printing speeds, shown at scales ranging from 0.5 mm to 2 mm, used to evaluate the effect of printing speed on surface morphology.

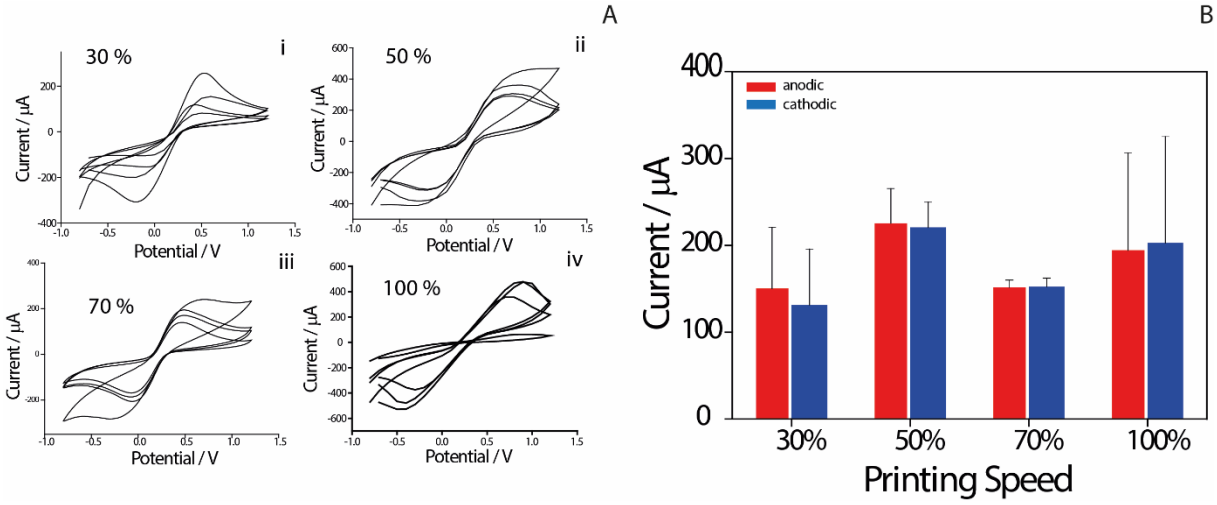

Figure S5. The influence of different 3D-printing speeds (30%, 50%, 70%, and 100%) was investigated in terms of: A) the consistency of electrochemical behavior observed in voltammograms, and B) the current intensity and reproducibility of the 3D-printed electrodes. CV experiments were performed for each printing speed using electrodes immersed in 1 mL of 5 mM potassium ferricyanide ($K_3Fe(CN)_6$) solution, in a scan rate of 0.05 $V \cdot s^{-1}$. The standard deviations of the current intensities correspond to measurements obtained from four 3D-printed electrodes of the same batch, fabricated at various printing speeds.

Table S1. The dimensions (mm), the conductive PLA filament needed (m) for the printing of six electrodes, the weight(g) and the cost of the 6 electrodes and in the last column is presented the cost per unit, i.e cost per unit (€).

Dimensions (mm)	Filament needed (m)	Printing time (min)	Weight (g)	Cost (€)	
6 replicates of 3D-pritned electrodes					**Cost per unit (€)**
2x2x30	0.34	14	1	0.10	0.02
4x2x30	0.64	30	1.92	0.19	0.03
6x2x30	1.16	48	3.46	0.35	0.06
8x2x30	1.56	66	4.54	0.45	0.08
10x2x30	1.92	78	5.76	0.58	0.10

Infill patterns optimization

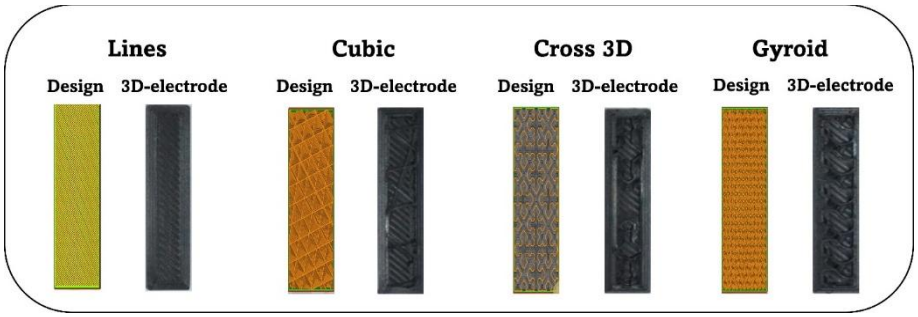

Figure S6. The 3D designs of various infill patterns—namely lines, cubic, cross-3D, and gyroid—were used for optimization studies, and appearance of the 3D electrodes that were printed based on these designs.

SEM characterization of 3D-printed electrodes with different infill patterns was performed to evaluate their effect on the electrode surface.

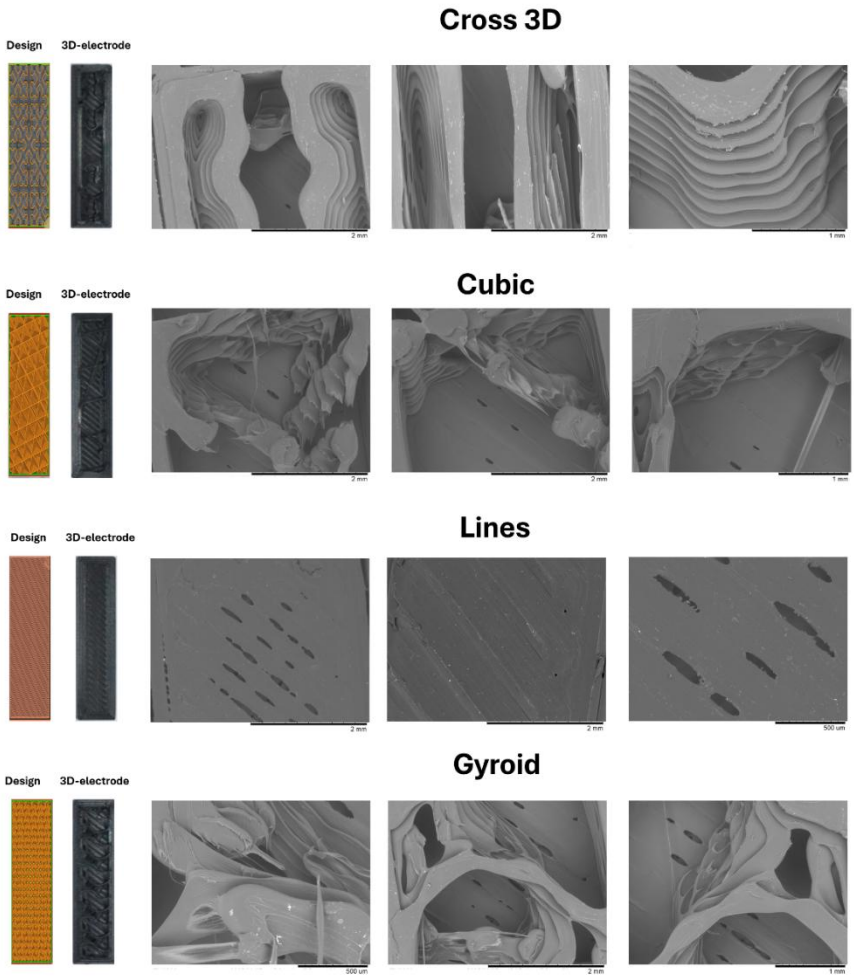

Figure S7. SEM micrographs were obtained for all the different patterns across the entire surface length of the electrodes. Infill patterns selected for evaluation based on the distinct morphological characteristics they impart to the 3D-printed electrodes. The tested infill patterns included cross 3D, cubic, lines, and gyroid, each applied to the electrode surface to assess their impact on structure and electrochemical performance.

Interestingly, our results revealed that the simplest surface pattern, based on a basic line architecture, provided the most reproducible electrochemical responses (Fig.3A). Although more complex infill patterns with increased surface roughness and cavities initially appeared promising due to higher current densities, they ultimately led to inconsistencies that negatively affected sensor performance. This outcome is consistent with observations in literature, where enhanced sensitivity is often offset by poor reproducibility due to irregular or non-uniform surface features.

Notably, despite the inherent design flexibility of 3D printing, most studies to date have continued to replicate conventional, flat electrode geometries, rather than fully leveraging the "freedom of design" offered by additive manufacturing. To truly harness the potential of 3D printing in electrochemical and electroanalytical applications, it is essential to move beyond conventional paradigms and focus on understanding and working within the constraints of printed materials.

In our study, the use of a simple linear infill pattern, while structurally modest, demonstrated superior repeatability and performance, reinforcing the idea that thoughtful, material-aware design is more impactful than mere complexity.

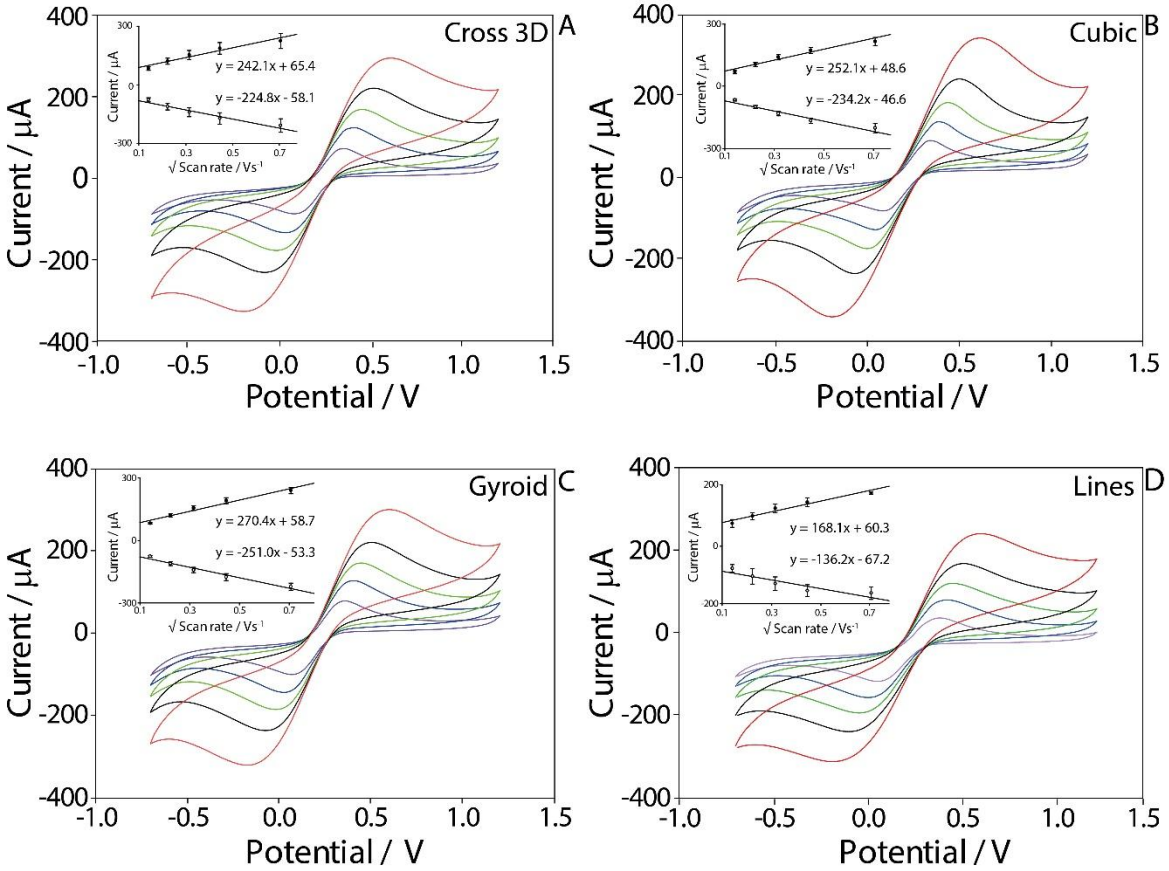

Figure S8. Optimization of the infill pattern evaluated for A) Cross 3D, B) Cubic, C) Gyroid and D) Lines patterns. CV experiments were recorded for each electrode infill pattern through the analysis of 1 mL of 5 mM $K_3Fe(CN)_6$ solution, using increasing scan rates from 0.02 to 0.5 Vs^{-1}. Inset: linearity among the intensity of the anodic (solid black circles) and cathodic (empty white

circles) and the square root of the tested scan rates. The experiments were performed in 6 replicates.

Reference Electrode investigation

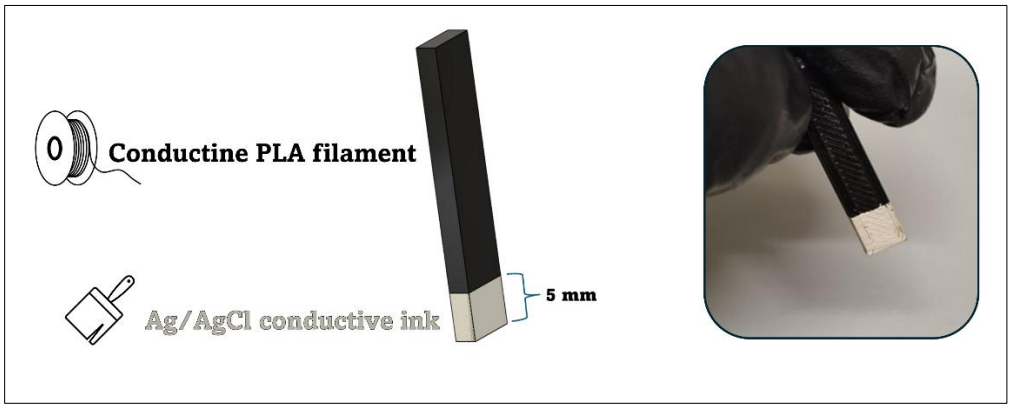

Figure S9. Reference electrode of the 3D-printed electrochemical consisted of conductive PLA filament and a single-pass thin layer of Ag/AgCl conductive ink.

Analytical performance of the 3D-printed electrochemical sensor: potassium ferricyanide as model target

After completing the optimization studies, the final 3D-printed three-electrode sensor was characterized using potassium ferricyanide at varying scan rates (Fig. S10A, S10B). Additionally, potassium ferricyanide was employed as a model target to construct a calibration curve in the concentration range of 0.05–1 mM. The system demonstrated good linearity, confirming its analytical performance (Fig. S10B).

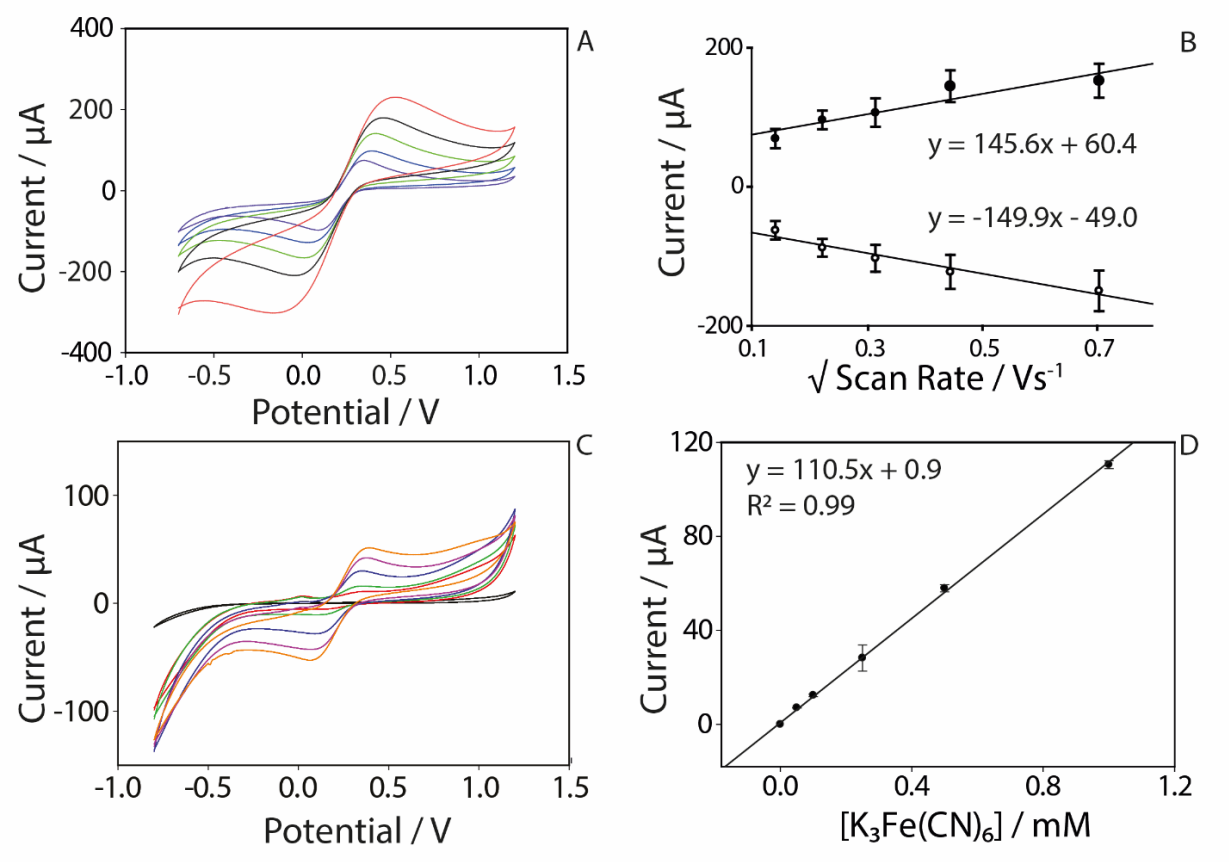

Figure S10. Evaluation of the final 3D-printed configuration with 6x2x30 mm dimensions and lines infill pattern. A) Cyclic voltammetric experiments were recorded through the analysis of 1 mL of 5 mM $K_3Fe(CN)_6$ solution, using increasing scan rates from 0.02 to 0.5 Vs^{-1}. B) Linearity among the intensity of the anodic (solid black circles) and cathodic (empty white circles) and the square root of the tested scan rates. C) Cyclic voltammetric experiments were recorded through the analysis of 1 mL of various $K_3Fe(CN)_6$ from 0.25-1 mM in a scan rate of 0.05 Vs^{-1}. D) Calibration curve obtained at increasing $K_3Fe(CN)_6$ concentrations from 0.05 to 1 mM.

Analytical performance of the 3D-printed electrochemical sensor: ascorbic acid as a proof of concept

Guideline for Non-Linear Baseline Correction of Voltammograms in PSTrace (PalmSens): To perform non-linear baseline correction, the raw voltammetric curve is first imported into PSTrace. From the menu, the *Curve Operations* option is opened, and *Non-linear baseline* is selected. The user then marks two edge points of the voltammogram with the cursor to define the

baseline range. Finally, by confirming with *OK*, the corrected voltammogram is generated and can be saved for further analysis.

The software allows selection of the polynomial order (2, 3, or 4) used for the baseline fitting. Polynomial 2 (quadratic) or 3 (cubic) is generally recommended, as these provide adequate correction of capacitive background while maintaining the integrity of the faradaic peaks. Higher polynomial orders (e.g., 4) may risk overfitting, potentially distorting the true electrochemical signal. Therefore, careful choice of polynomial degree is essential to ensure reliable and reproducible analysis.

This simple function facilitates the analytical characterization of the sensor enabling the same baseline for all the peaks.

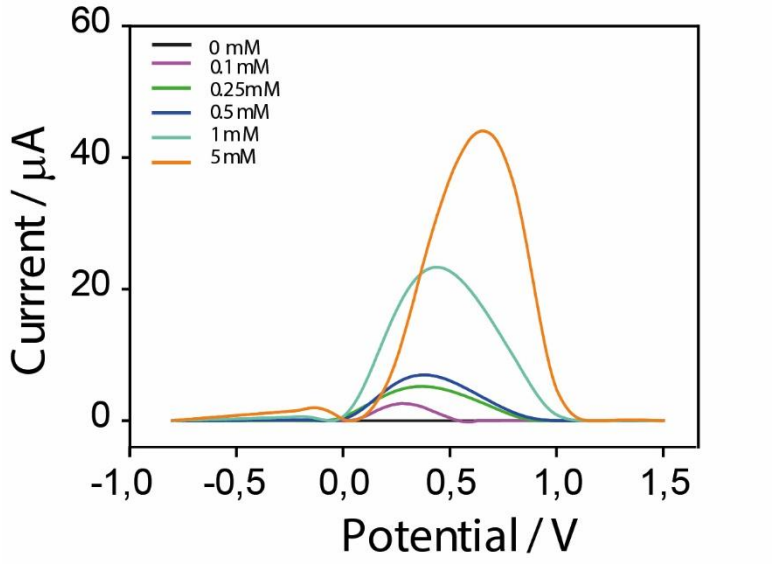

Figure S11: Voltammetric curves obtained for increasing ascorbic acid concentrations, 0.1-5 mM, in 10 mM of acetate buffer at pH 4.7. The black like represents the acetate buffer, that served as a blank sample, used to prepare the ascorbic calibrators. The 3D device responses were recorded in LSV in the potential range from -0.1 to +1.4 V at 0.05 V/s.

Real sample application

The analysis of real samples was conducted by inserting the trident-shaped fully 3D-printed sensor into the fruit and vegetables. Measurements were then performed as described in the main

manuscript. A comparison was also made with the standard Liquid Chromatography-Tandem Mass Spectrometry (LC-MS/MS) method.

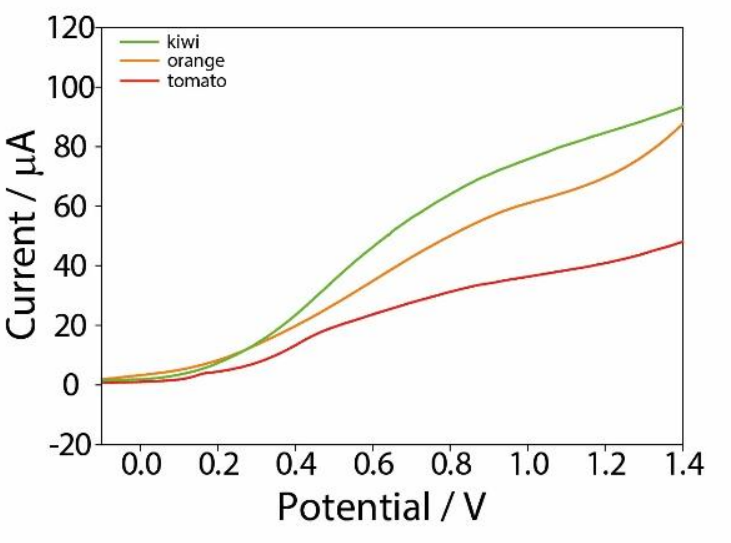

Figure S12: Voltammograms obtained using the fully 3D-printed device in the inside of the orange sample (orange line), tomato sample (red line) and kiwi (green line). The 3D device responses were recorded in LSV in the potential range from -0.1 to +1.4 V at 0.05 V/s. The experiments were performed in three replicates.

Table S2. Application of the fully 3D-printed sensor for ascorbic acid (AA) detection in real fruit and vegetable samples, and its comparison with the gold-standard LC-MS/MS method. Experiments were performed in triplicate for both the 3D-printed sensors and for the LC-MS/MS.

Samples	**Fully 3D-printed sensor**	**LC-MS/MS**
	[AA] / mM	
orange	0.91 ± 0.02	0.90 ± 0.09
tomato	0.73 ± 0.06	0.63 ± 0.01
kiwi	2.47 ± 0.20	2.58 ± 0.03

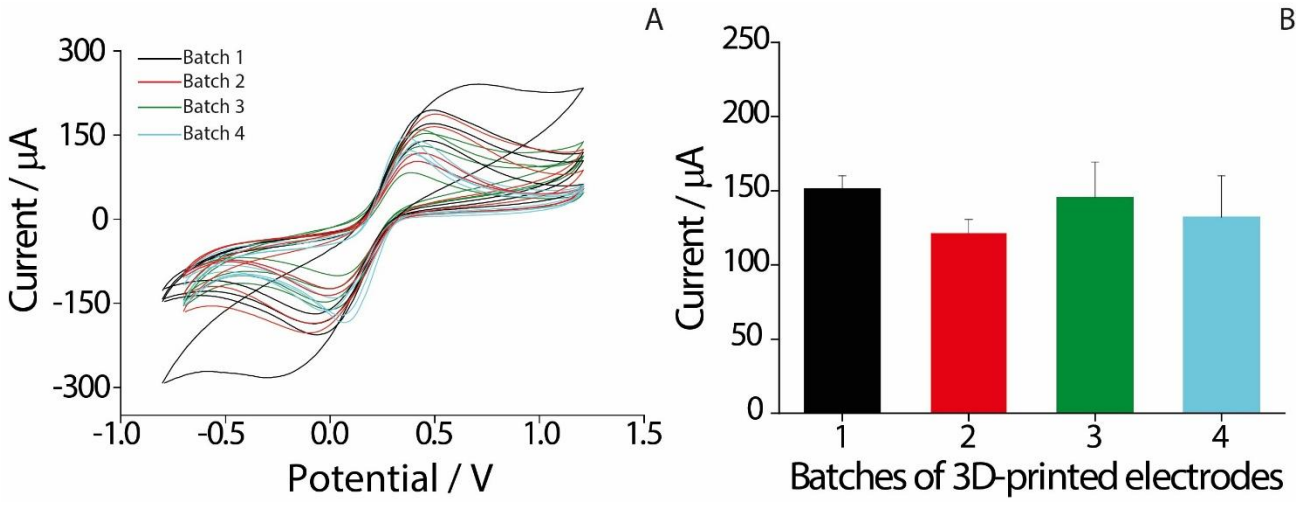

Figure S13. Electrochemical performance of 3D-printed electrodes from four different batches. (A) Voltammograms obtained from electrodes in each batch, demonstrating overall consistency with minor variations. (B) Peak current intensities and standard deviations for each batch, highlighting the reproducibility of the fabrication process.

Reusability potential of the fully 3D-printed device

After the initial use, the 3D-printed electrodes were thoroughly rinsed with running water to remove any residual material, then dried to prepare them for the next cycle. Following this, the electrodes were pre-treated again with a 0.5 M NaOH solution to help remove any contaminants or buildup from previous use. After the pre-treatment step, the electrodes were rinsed again and then used for ascorbic acid detection as described in the Experimental section. Each cycle involved a complete process, including cleaning, pre-treatment, and subsequent analyte detection.

To assess the reusability of the electrodes, up to three reuse cycles were performed, with ascorbic acid detection carried out at three different concentrations: 0.25 mM, 0.5 mM, and 1 mM. The results clearly demonstrate the electrodes' excellent reusability, as they maintained reliable performance across all three cycles, indicating their potential for multiple uses without significant loss of efficiency or sensitivity.

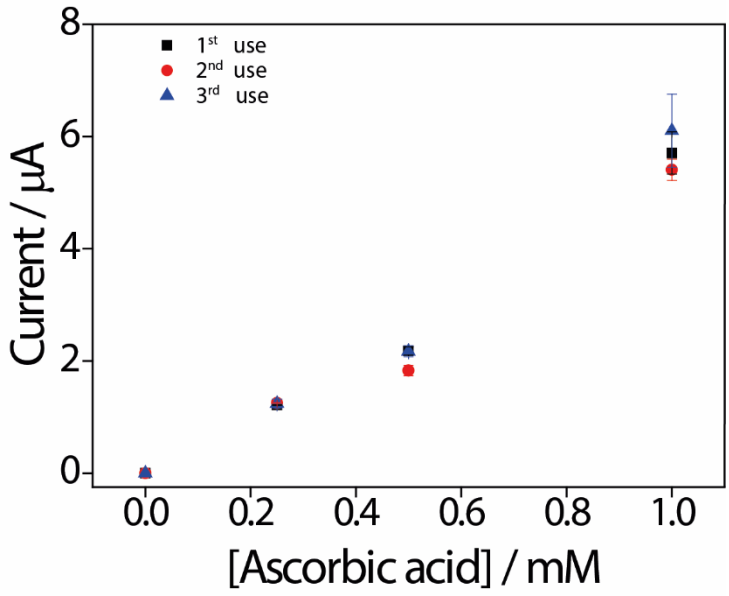

Figure S14. Robustness and stability of 3D-printed electrodes. Electrochemical detection of ascorbic acid at three concentration levels (0.25 mM, 0.5 mM, and 1 mM) using 3D-printed electrodes after up to three reuse cycles, each consisting of a cleaning, pretreatment, and analyte detection step.